

MODIS Cloud-Top Property Refinements for Collection 6

BRYAN A. BAUM, W. PAUL MENZEL, RICHARD A. FREY, DAVID C. TOBIN, ROBERT E. HOLZ,
AND STEVE A. ACKERMAN

Space Science and Engineering Center, University of Wisconsin—Madison, Madison, Wisconsin

ANDREW K. HEIDINGER

NOAA/NESDIS/Center for Satellite Applications and Research, Madison, Wisconsin

PING YANG

Texas A&M University, College Station, Texas

(Manuscript received 20 September 2011, in final form 23 January 2012)

ABSTRACT

This paper summarizes the Collection-6 refinements in the Moderate Resolution Imaging Spectroradiometer (MODIS) operational cloud-top properties algorithm. The focus is on calibration improvements and on cloud macrophysical properties including cloud-top pressure–temperature–height and cloud thermodynamic phase. The cloud phase is based solely on infrared band measurements. In addition, new parameters will be provided in Collection 6, including cloud-top height and a flag for clouds near the tropopause. The cloud parameters are improved primarily through 1) improved knowledge of the spectral response functions for the MODIS 15- μm carbon dioxide bands gleaned from comparison of coincident MODIS and Atmospheric Infrared Sounder (AIRS) radiance measurements and 2) continual comparison of global MODIS and *Cloud–Aerosol Lidar and Infrared Pathfinder Satellite Observations (CALIPSO)* instantaneous cloud products throughout the course of algorithm refinement. Whereas the cloud-top macrophysical parameters were provided through Collection 5 solely at 5-km spatial resolution, these parameters will be available additionally at 1-km spatial resolution in Collection 6.

1. Introduction

An objective of the National Aeronautics and Space Administration (NASA) Earth Observation System is to develop data products of the highest possible accuracy and reliability from sensors on the *Aqua* and *Terra* platforms; the data products should be of sufficient quality to be considered as “climate data records.” To this end, a number of improvements to the Moderate Resolution Imaging Spectroradiometer (MODIS) Collection-6 cloud-products algorithm are being incorporated that will improve the record of global cloud-top properties—to be specific, cloud-top temperature and pressure and the discrimination of cloud thermodynamic phase using infrared (IR) window bands. The cloud-top parameters

(pressure, temperature, and IR phase) provided in Collection 5 (and earlier collections) are for 5×5 pixel arrays (approximately 5-km resolution at nadir). These products will continue in Collection 6, but a new focus is to provide these cloud products at 1-km spatial resolution. In addition, new parameters include cloud-top height (CTH) and a flag for clouds in the upper troposphere/lower stratosphere (UT/LS), that is, a cloud within 2 km of the tropopause. The purpose of this paper is to document the improvements that had positive impacts on the derivation of Collection-6 cloud-top macrophysical parameters.

The Collection-6 refinement activity has benefited greatly from the ability to compare MODIS radiance data and products acquired with various sensors that compose the A-Train. Major impact has come from 1) improved knowledge of the spectral response functions for the MODIS 15- μm carbon dioxide (CO_2) bands obtained through comparison with Atmospheric Infrared Sounder (AIRS) high-spectral-resolution infrared data and

Corresponding author address: Dr. Bryan A. Baum, Space Science and Engineering Center, University of Wisconsin—Madison, 1225 W. Dayton St., Madison, WI 53706.
E-mail: bryan.baum@ssec.wisc.edu

2) comparison of global MODIS products (passive sensor) with those from the Cloud–Aerosol Lidar with Orthogonal Polarization (CALIOP; active lidar) on the *Cloud–Aerosol Lidar and Infrared Pathfinder Satellite Observation (CALIPSO)* satellite platform throughout the course of algorithm refinement. These topics will be discussed in detail in section 3.

The algorithm refinements for Collection 6 include changes to the radiative transfer model, such as using ozone profiles provided in the meteorological products rather than from climatological values, using surface emissivity maps (Seemann et al. 2008), and incorporating shifts in spectral response functions for three of the 15- μm CO₂ bands (bands 34, 35, and 36 at 13.6, 13.9, and 14.2 μm , respectively). Additional algorithm changes include applying the CO₂-slicing method only to ice clouds as determined by cloud emissivity ratios using the 7.3-, 8.5-, 11-, and 12- μm bands (i.e., bands 28, 29, 31, and 32, respectively) and inferring low-level cloud heights over water through a latitude-dependent 11- μm brightness temperature (BT) lapse rate. The lapse rates used for marine clouds are developed from collocated MODIS-observed BTs, *CALIPSO* low-level cloud heights, and sea surface temperatures, with a different set of lapse rates determined for each month for a full year of data from July of 2007 to June of 2008. The IR cloud-phase method was modified significantly to incorporate recent work involving cloud emissivity ratios (Heidinger and Pavolonis 2009; Heidinger et al. 2010; Pavolonis 2010). The approach requires a forward radiative transfer model to calculate clear-sky radiances from an input set of temperature, humidity, and ozone profiles provided by a gridded meteorological product. In addition, the cloud mask (known as MYD35) that identifies pixels for input to cloud-products algorithms has been updated. Improvements include use of normalized difference vegetation index (NDVI) fields to enhance knowledge of expected surface reflectances and to better define certain cloud-test thresholds. Nighttime clear-sky and cloud discrimination was improved by use of dynamic thresholds in the brightness temperature difference [BTD(3.9–11 μm)] cloud test. Collocated CALIOP data were used to develop thresholds as functions of water vapor loading for both water and land surfaces. Details of these and other changes are found in section 3a. The Collection-5 software for cloud-top parameters was upgraded to include a new processing framework. This new Collection-6 software framework enables the production of cloud properties at 1-km spatial resolution.

Section 2 describes the datasets and models used in this study, and section 3 provides a description of the various algorithm refinements. Section 4 shows selected

global results that compare Collection 5 with anticipated Collection-6 results. A comparison of MODIS with *CALIPSO* global cloud heights is discussed in section 5, and section 6 provides a summary and conclusions.

2. Data and models

a. AIRS

The AIRS is a hyperspectral, scanning infrared sounder that measures emitted infrared radiation in 2378 spectral channels spanning the range from 3.7 to 15 μm (Aumann et al. 2003). The AIRS operates on the NASA *Aqua* platform and is part of the A-Train constellation of sensors. The spatial resolution of a field of view (FOV) at nadir is 13.5 km, and complete global coverage is attained daily using cross-track scanning. Because of its high spectral resolution in the infrared and its excellent absolute accuracy, AIRS retrieval algorithms are able to obtain vertical profiles of atmospheric temperature, moisture, and trace gases (Chahine et al. 2006; Susskind et al. 2003). Tobin et al. (2006a) describe an absolute radiometric comparison of AIRS with the aircraft-based Scanning High-Resolution Interferometer Sounder (HIS). In addition, two studies comparing the AIRS level-1B (L1B) radiances with those obtained from the AIRS clear-sky forward model [the Stand-Alone AIRS Radiative Transfer Algorithm (SARTA)] indicate a relative accuracy of about 0.2 K (Tobin et al. 2006b; Strow et al. 2006). Tobin et al. (2006b) assume a circular shape for the AIRS FOV since the point of the comparisons is to assess the radiometric bias, which can be done with uniform scenes that are insensitive to the details of the FOV shape. Extension of this approach to nonuniform scenes could be made using the AIRS spatial response function obtained from pre-launch calibration activities, as reported in Schreier et al. (2010).

b. MODIS

MODIS is a 36-channel whisk-broom scanning radiometer currently flying on the NASA *Terra* and *Aqua* platforms (Salomonson et al. 1989). Launched in December of 1999, the *Terra* platform is in a daytime descending orbit with an equatorial crossing of 1030 local solar time (LST). The *Aqua* platform, launched in May of 2002, is in a daytime ascending orbit at 1330 LST. The equatorial crossing times have been held constant over the years for both platforms. The MODIS sensor has four focal planes that cover the spectral range 0.42–14.24 μm , with each spectral band defined by an interference filter. MODIS has several onboard instruments to provide information for evaluating and

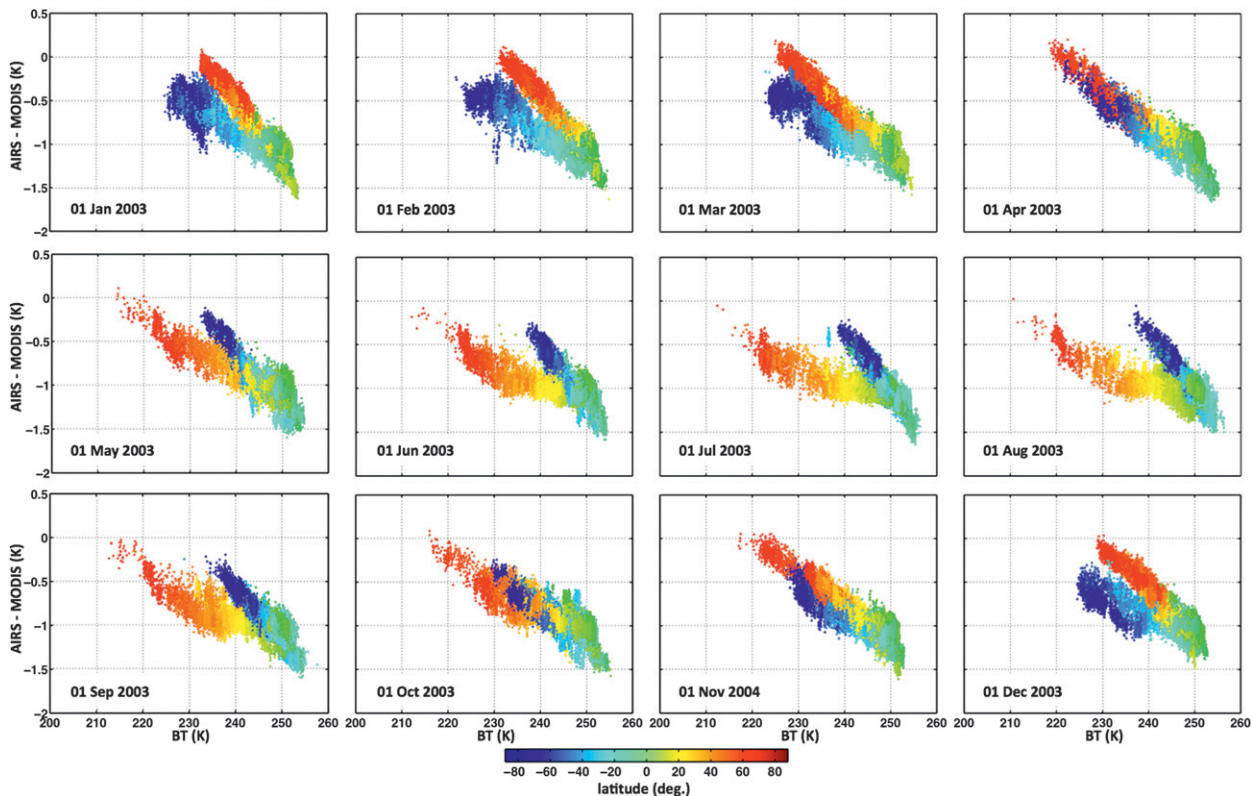


FIG. 1. The (AIRS–MODIS) BTDs shown as a function of 11- μm scene BT. The (AIRS–MODIS) BTDs are calculated with AIRS data convolved using the nominal MODIS SRF (i.e., unshifted). The BTDs are color coded as a function of latitude, with red points coming from the high latitudes in the Northern Hemisphere and blue points coming from high latitudes in the Southern Hemisphere.

monitoring on-orbit performance and calibration (e.g., Xiong et al. 2009). Thermal spectral bands are monitored and calibrated with an onboard blackbody. Although a characterization of the spectral response functions has been provided for each of the MODIS bands both pre- and postlaunch, Tobin et al. (2006b) have provided a way to gain further insight into the IR bands by comparing MODIS radiance measurements with those from AIRS as shown below. The MODIS products used in this study include the Collection-5 1-km spectral radiance data (MYD021KM for *Aqua*), geolocation data (MYD04 for *Aqua*), and the cloud properties at 5-km resolution (MYD06 for *Aqua*).

USE OF AIRS AND MODIS TO EVALUATE MODIS SPECTRAL RESPONSE FUNCTIONS

Tobin et al. (2006b) describe an approach for evaluating MODIS infrared-band spectral response functions (SRFs) by comparing AIRS and MODIS radiance data. In the current work, the exploratory study of Tobin et al. (2006b) is expanded from evaluation of one full orbit to analyzing collocated AIRS and MODIS data for the first

day of every month in 2003 (except November, for which 2004 data were used because of an issue with the AIRS sensor in November of 2003). The MODIS Collection-5 L1B radiances and 1-km geolocation data were used, and the AIRS L1B radiances were generated using version 5.0.0.0. Most but not all of the 2378 AIRS spectral channels were used (some of the channels were not recommended for use by the AIRS science team and were excluded in level-2 processing).

The SRF evaluation process begins with convolving the high-spectral-resolution AIRS data with a given MODIS band's SRF. Then, the 1-km-spatial-resolution MODIS data are collocated with an individual lower-spatial-resolution AIRS FOV (assumed to be circular) and are averaged. For comparison purposes, spatially uniform scenes are used. Only those AIRS FOVs for which the standard deviation of the collocated MODIS BTs is less than or equal to 0.2 K are selected; that is, the data are filtered for uniform scenes with low variability. Figure 1 provides (AIRS–MODIS) BTDs for MODIS band 35 (13.9 μm) for the first day of every month. The BTDs are color coded as a function of latitude, with red

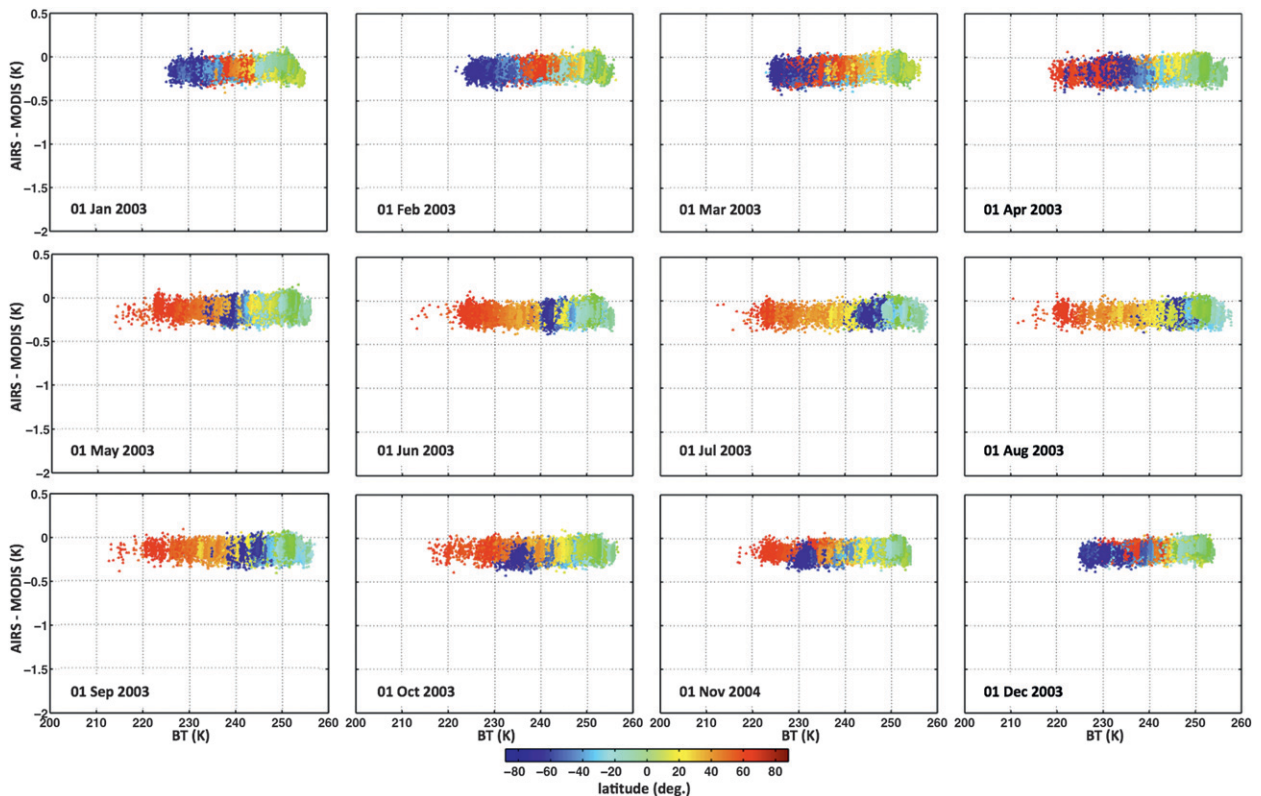


FIG. 2. As in Fig. 1, but the AIRS data are convolved after shifting the nominal MODIS SRF by 0.8 cm^{-1} .

points coming from high latitudes in the Northern Hemisphere, green points coming from the tropics (low latitudes), and blue points coming from high latitudes in the Southern Hemisphere. The BTDs in the tropics remain fixed at approximately -1.5 K , but the higher-latitude BTDs change with the season. The AIRS–MODIS BTDs are shown for uniform scenes, but one might expect that were all scenes to be included then the bias would not change but the scatter would increase.

Tobin et al. (2006b) suggested that a slight shift in the MODIS spectral response functions could mitigate this effect. For MODIS band 35 they suggested shifting the MODIS SRF by 0.8 cm^{-1} ; the reanalyzed data with the suggested SRF shift for MODIS band 35 are shown in Fig. 2. Note that applying the correction to the BTDs reduces the latitudinal differences; the lower latitudes decrease from 1.5 to 0.2 K . In addition, the BT differences are now consistent from month to month. A single small shift in the SRF has largely eradicated the AIRS–MODIS BT latitudinal and seasonal differences. This finding is also the primary reason why Collection-6 cloud products will show so much improvement in determining optically thin high-level cloud heights, so much so that products can now be generated at 1-km resolution.

c. CALIPSO

The *CALIPSO* satellite platform carries several instruments, among which is a near-nadir-viewing lidar called CALIOP (Winker et al. 2007, 2009). *CALIPSO* flies in formation with NASA's Earth Observing System *Aqua* platform and is part of the A-Train suite of sensors. CALIOP takes data at 532 and 1064 nm. The CALIOP 532-nm channel is capable of measuring the linear polarization state of the lidar returns. The CALIOP lidar depolarization ratio contains information about aerosol and cloud properties.

d. Radiative transfer model and atmospheric profiles

Clear-sky radiances are calculated with the 101-level Pressure-Layer Fast Algorithm for Atmospheric Transmittance (PFAAST; Strow et al. 2003) model. This model requires as input a set of temperature, moisture, and ozone profiles, which are provided from gridded meteorological products from the National Centers for Environmental Prediction Global Data Assimilation System (GDAS; Derber et al. 1991). The temperature and water vapor profiles are provided every 6 h at 25-hPa intervals from 1000 to 900 hPa, at 50-hPa intervals from 900 to 100 hPa, and at 70, 50, 30, 20, and 10 hPa.

The tropopause is defined as the pressure level that has the coldest temperature between 100 and 400 hPa with the caveat that if isothermal conditions exist as the pressure increases from 100 hPa, the tropopause level is chosen where the profile begins to warm.

Through Collection 5, climatological ozone profiles were used for clear-sky calculations. Because ozone profiles are provided in GDAS at pressure levels between 10 and 100 hPa, which are most important for clear-sky calculations involving the 15- μm CO_2 bands, the decision was made to use these for Collection 6, thereby making the calculations more consistent with the GDAS. The band coefficients in the radiative transfer model were recalculated to incorporate the shifted spectral response functions. The radiative transfer model now makes use of surface spectral emissivity maps (Seemann et al. 2008). To be clear, the small shifts in the SRFs affect the radiance calculations in the radiative transfer model; the MODIS radiances measurements remain the same.

3. Algorithm refinements

a. MODIS cloud mask updates for Collection 6

Several updates to the MODIS cloud mask, for both *Aqua* and *Terra*, have been included in the Collection-6 data reprocessing effort. The revised cloud mask builds on improvements made for Collection 5 (Frey et al. 2008) and experience gained from validation of MOD35 cloud-detection results through intercomparison with those from ground, aircraft, and satellite measurements (Ackerman et al. 2008).

Improvements include the following. NDVI background maps at 1-min spatial resolution and collected over 16 days (Moody et al. 2005) are used in daytime land scenes. Band-1 (0.67 μm) reflectance cloud-test thresholds were derived as functions of background NDVI and scattering angle, replacing the static thresholds that were used in earlier versions. In the same way, band-8 (0.412 μm) cloud-test thresholds are derived for use in arid regions, defined as an NDVI background value of less than 0.25. A form of the 0.86/0.67- μm reflectance-ratio (global environmental monitoring index; Pinty and Verstraete 1992) cloud test is also defined as a function of NDVI background for use in deserts. In addition, the desert processing path in the MOD35 algorithm is defined as a background NDVI < 0.3, rather than from various indices in a static ecosystem map. Taken together, these changes reduce the number of pixels processed as “desert,” decrease the dependence on clear-sky restoral tests (where an initial cloudy classification is changed to clear), and reduce the number of

“probably clear” and “probably cloudy” designations in vegetated and semiarid locales.

For nighttime land scenes, a new BT(11–3.9 μm) cloud test employs thresholds as a function of total precipitable water from model output data (GDAS). A regression relationship was built based on collocated CALIOP (to discriminate between clear and cloudy skies) and MODIS observed BTs. This test enhances the detection of transmissive cirrus and reduces the number of probably cloudy results in clear-sky conditions, especially in humid tropical locations such as the Amazon basin. A similar nighttime ocean test is also new for Collection 6. Detection of low-level water-phase clouds and transmissive cirrus is enhanced.

For ocean regions, a new sea surface temperature (SST) test is included in which a SST is calculated and compared with ancillary data. Cloud is assumed (0.5 confidence of clear sky) if (ancillary SST – calculated SST) > 2.5 K.

Other enhancements include expanded airborne dust tests, now performed during day and night, and over land and water surfaces; a new smoke/pollution test for daytime water surfaces; and addition of a cloud adjacency flag to indicate pixels that immediately adjoin cloudy or probably cloudy pixels.

b. Infrared thermodynamic cloud phase

Through MODIS Collection 5, the IR-thermodynamic-cloud-phase product (Platnick et al. 2003) has been based on analysis of 8.5- and 11- μm BTs in 5×5 pixel arrays where the radiances for the cloudy pixels are averaged to reduce radiometric noise; the following classes were given: ice, water, mixed phase, and uncertain (Platnick et al. 2003). Recent studies demonstrate the strengths and limitations of this product (Cho et al. 2009; Nasiri and Kahn 2008). Two primary limitations are that 1) optically thin cirrus may not be classified as ice phase and 2) supercooled-water or mixed-phase cloud identification is problematic. To mitigate the labeling of optically thin cirrus as being other than ice phase, the method is enhanced by using cloud emissivity ratios, as discussed in Heidinger and Pavolonis (2009), Heidinger et al. (2010), and Pavolonis (2010).

The radiance at the top of the atmosphere (TOA) can be approximated as

$$I = (1 - \varepsilon)(I_{\text{clr}} - I_{\text{ac}}) + I_{\text{ac}} + T_{\text{ac}}\varepsilon B(T_{\text{eff}}), \quad (1)$$

where I is the TOA radiance, I_{clr} is the TOA clear-sky radiance, I_{ac} is the above-cloud emission contribution from the atmospheric layer, T_{ac} is the above-cloud transmittance, and $B(T_{\text{eff}})$ indicates the blackbody radiation at the effective temperature T_{eff} of the cloud.

From Eq. (1), the cloud emissivity for a single band is given by

$$\varepsilon = \frac{(I - I_{\text{clr}})}{[I_{\text{ac}} + T_{\text{ac}}B(T_{\text{eff}}) - I_{\text{clr}}]} \quad (2)$$

Further, the cloud emissivity for multiple bands can be related through the use of the so-called β parameter (Parol et al. 1991):

$$\beta = \frac{\ln(1 - \varepsilon_y)}{\ln(1 - \varepsilon_x)} \quad (3)$$

where x and y refer to the two bands used to compute the ratio. The importance of the β parameter is that it merges measured satellite radiances with clear-sky radiances provided by either a radiative transfer model or from pixels determined to be clear sky through use of a cloud-clearing approach. By accounting for the clear-sky radiance, the influence of the surface is decreased from that found in the measured BTDs employed in the Collection-5 (and earlier) thermodynamic-phase method.

Because the IR thermodynamic phase runs separately from the CTH algorithm, the CTH is not known when computing the cloud emissivity in Eq. (2). As shown in Heidinger et al. (2010), the variation of cloud emissivity with cloud height is small for cirrus clouds through the upper troposphere using IR-window bands. The reasoning for choosing the tropopause temperature is described in Pavolonis (2010) and is summarized here. An emissivity is simply a ratio of two radiance differences. The cold temperature point is chosen to ensure that emissivities are always less than unity. This emissivity is treated as a metric, and an empirically derived threshold is placed on it. The benefit of this metric is that it accounts for clear-sky variations in the presence of cirrus clouds and approximates the true cloud emissivity for high clouds. Note that this use of emissivity ratios (i.e., β) is employed primarily to improve discrimination of optically thin high-level clouds as being ice; it is not very useful to improve discrimination of supercooled water clouds. Therefore, the use of the tropopause height as the reference level for high clouds is adequate for the qualitative IR-phase application.

As a complement to window bands used in the cloud-emissivity method, IR absorption bands provide useful information about the cloud height (Heidinger et al. 2010). For MODIS, measurements are available in both the broad water vapor and CO_2 absorption regions. The $7.3\text{-}\mu\text{m}$ band is used to further discriminate between optically thin ice clouds and low-level clouds; this band is chosen instead of one of the $15\text{-}\mu\text{m}$ bands because it is less affected by detector striping. Use of the tropopause

reference for the cloud-emissivity calculation maintains the unique relative signatures offered by the $7.3\text{-}\mu\text{m}$ band. For lower-level clouds, the emissivities inferred from use of the tropopause pressure are significantly biased from their true value. The relative emissivity ratio differences remain, however, and provide the needed skill in phase separation.

Figure 3 is a flowchart of the refined IR-thermodynamic-phase method over ocean (Fig. 3a) and land (Fig. 3b). Three different band pairs are used: 7.3 and $11\ \mu\text{m}$, 8.5 and $11\ \mu\text{m}$, and 11 and $12\ \mu\text{m}$. The $8.5\text{--}11\text{-}\mu\text{m}$ band pair is primarily sensitive to ice-phase clouds, and the information content in the $11\text{--}12\text{-}\mu\text{m}$ band pair is related to cloud opacity. The $7.3\text{--}11\text{-}\mu\text{m}$ pair helps to separate high clouds from low clouds. The following example demonstrates how the use of these band pairs improves the identification of optically thin ice clouds.

Figure 4 illustrates the utility of incorporating the β parameter for cloud phase for a MODIS granule collected at 1630 UTC 28 August 2006 over the northern Atlantic Ocean. In the false-color image (Fig. 4a), ocean is dark, land is green, cirrus is blue, optically thick ice (southern tip of Greenland) and optically thick ice clouds are magenta, and low clouds are yellow/white. Figure 4b shows results obtained from the Collection-5 MYD06 product for IR phase at 5-km resolution, and Fig. 4c shows the same set of IR-phase tests applied at 1-km spatial resolution. For the Collection-5 results, the “mixed phase” pixels are merged into the “uncertain” category. The reason for this is that comparisons of the MODIS IR phase with the CALIOP version-3 cloud phase (see section 5 below) indicate that the MODIS IR-phase algorithm cannot unambiguously identify the presence of supercooled water or mixed-phase clouds. The planned Collection-6 discrimination of ice-phase clouds is improved in the results shown in Fig. 4d.

A Collection-6 IR-thermodynamic-phase product will be provided at both 1- and 5-km resolution, and at both spatial resolutions the mixed-phase category is being eliminated as a separate category so that results will be provided as ice, water, or uncertain. The improved cloud-phase product described above will be provided only at 1-km resolution. The 5-km phase product will continue to be provided for continuity, but the 1-km product is the focus of Collection-6 (and future) efforts.

c. Refinement of cloud-height algorithms

1) REFINEMENT OF CO_2 SLICING FOR MID- TO HIGH-LEVEL CLOUDS

Menzel et al. (2008) provide a thorough description of the CO_2 -slicing method used in MODIS Collection 5. To summarize the method, cloud-top pressure and effective

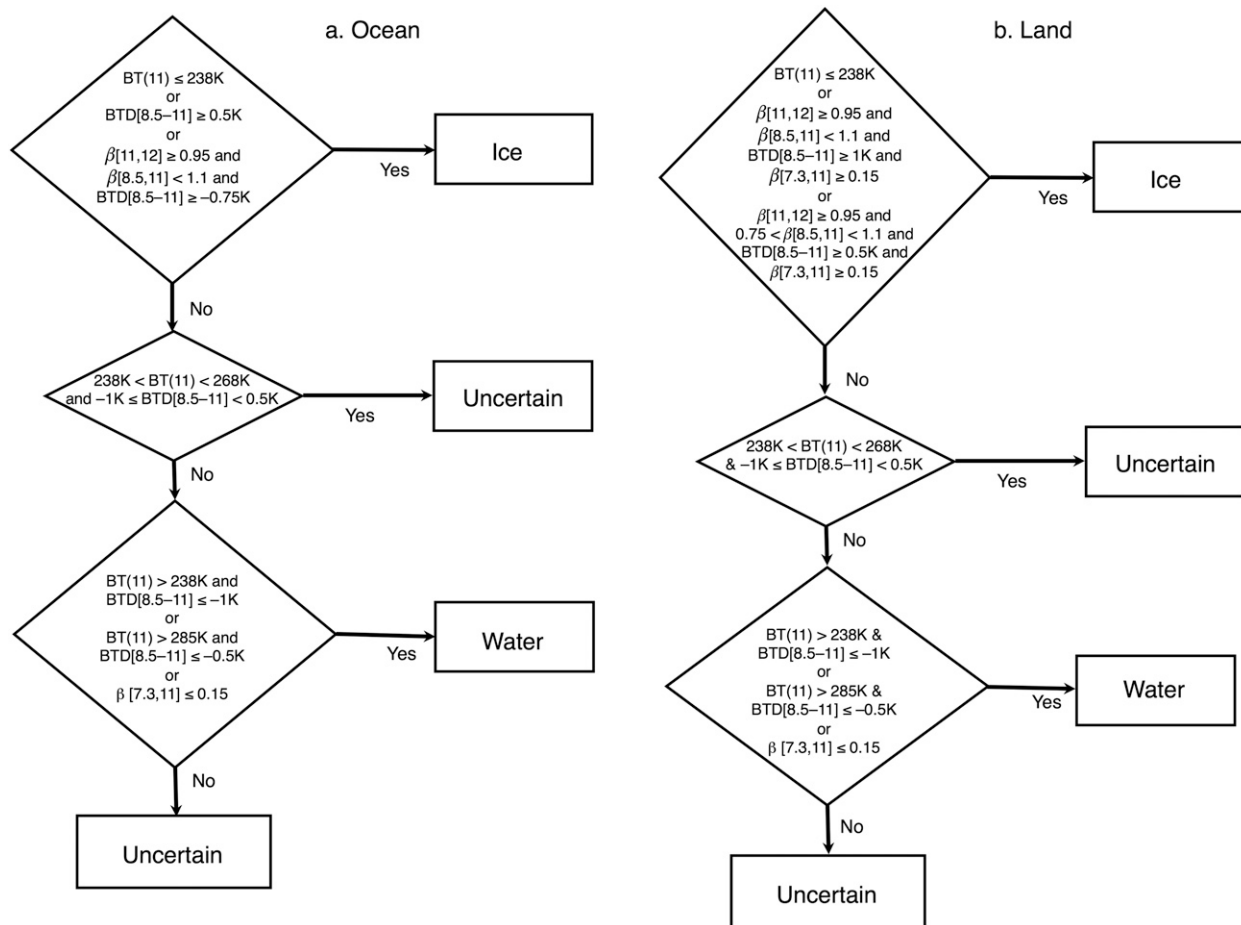


FIG. 3. MODIS Collection-6 tests for IR cloud thermodynamic phase over (a) ocean and (b) land.

cloud amount (defined as cloud fraction multiplied by cloud emissivity) are derived for mid- to high-level clouds using the 15- μm channels in the CO_2 absorption band. If a solution is not found using this approach, a default solution is obtained using the 11- μm data and assuming that a low-level opaque water cloud is present. For MODIS through Collection 5, cloud-top properties are produced solely for 5×5 pixel arrays where the radiances for the cloudy pixels are averaged to reduce radiometric noise. The MODIS cloud pressure is converted to cloud temperature (and later in Collection 6 to cloud height) through the use of gridded meteorological products provided by the GDAS model output. Calculated clear-sky radiances are derived with PFAAST (Strow et al. 2003) using the GDAS temperature, moisture, and ozone profiles. To mitigate height assignment errors caused by differences between model-derived and measured clear-sky radiances, a radiance bias adjustment is incorporated. Cloud properties are derived similarly for both daytime and nighttime data because the IR method is independent of solar illumination.

What follow below are refinements incorporated into the Collection-6 CO_2 -slicing algorithm:

- 1) *Cloud detection thresholds for MODIS band radiances are decreased.* The pixel must have a cloud signal (clear-sky calculated minus cloudy-sky measured radiance) above a predefined threshold for application of CO_2 slicing. For Collection 6, the band radiance thresholds are lowered to 1.25, 1.00, 1.00, and 0.75 $\text{mW m}^{-2} \text{sr}^{-1} \text{cm}$ for bands 36–33 at 14.2, 13.9, 13.6, and 13.3 μm , respectively, thus forcing more CO_2 -slicing solutions for high thin clouds. For Collection 5, the radiance thresholds for the same bands were 2, 3, 5, and 5 $\text{mW m}^{-2} \text{sr}^{-1} \text{cm}$. The threshold for band 31 (11 μm) remained the same at 0.5 $\text{mW m}^{-2} \text{sr}^{-1} \text{cm}$ for both Collections 5 and 6.
- 2) *The GDAS stratospheric ozone profile are used in the stratosphere, rather than climatological values.* GDAS ozone at pressure levels between 10 and 100 hPa is now used for radiance calculations rather than ozone climatological profiles.

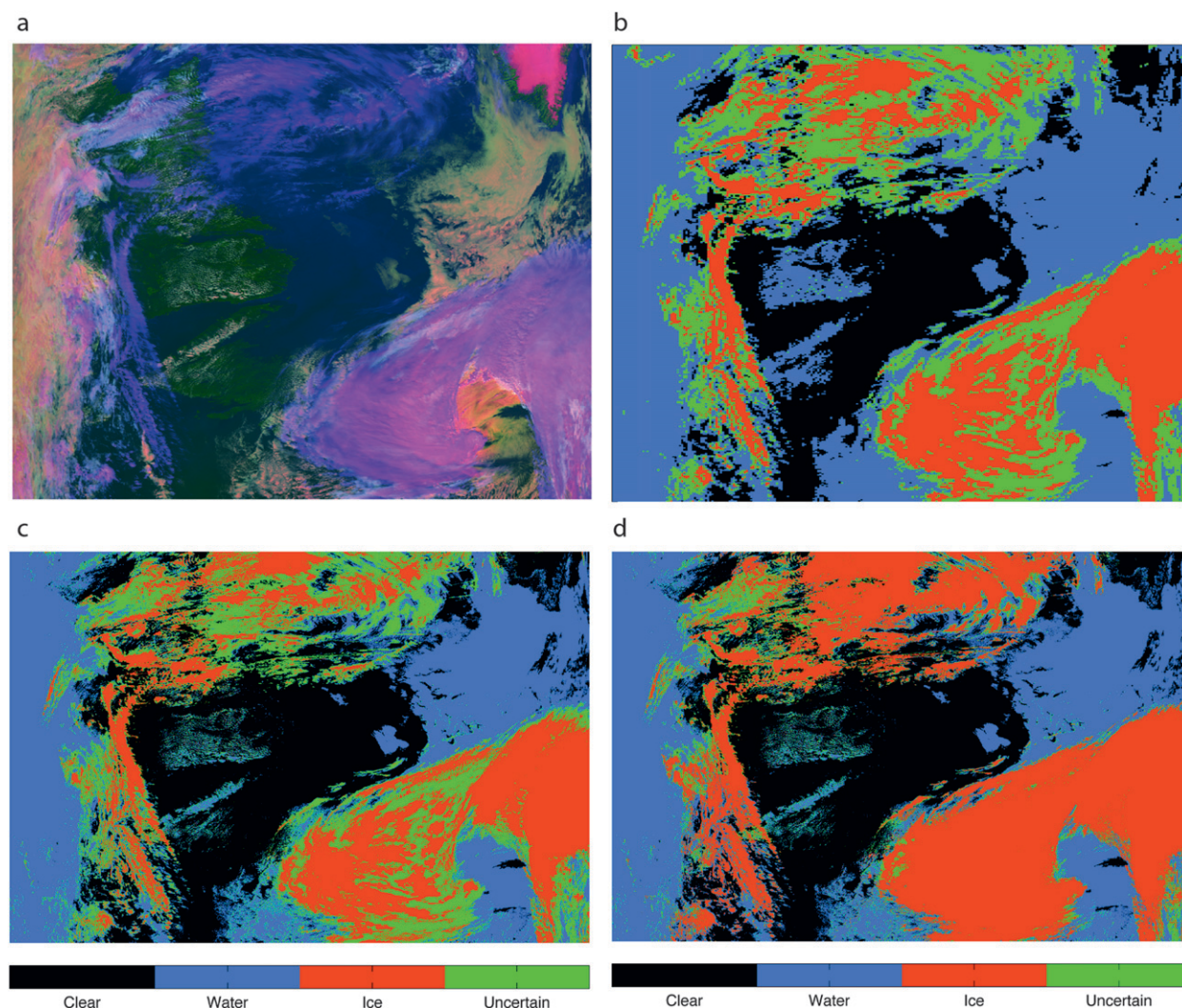


FIG. 4. Results of IR cloud phase for a MODIS granule at 1630 UTC 28 Aug 2006, over the northern Atlantic Ocean. (a) A false-color image (red, $0.65 \mu\text{m}$; green, $2.15 \mu\text{m}$; blue, $11 \mu\text{m}$ reversed) in which ocean is dark, land is green, cirrus is blue, optically thick ice cloud is magenta, and low clouds are yellow/white. (b) Collection-5 IR-phase results at 5-km resolution, (c) Collection-5 IR-phase algorithm applied at 1-km spatial resolution, and (d) the improved IR cloud phase. For the Collection-5 results, the mixed-phase pixels are merged into the uncertain category, as will be done with Collection 6.

- 3) *False high-cloud solutions located at the tropopause are reduced.* The CO_2 -slicing algorithm must converge at a pressure level at or below the tropopause.
- 4) *CO_2 slicing is limited to ice clouds using cloud emissivity ratios.* The emissivity of the cloud is assumed to be the same at both wavelengths, which is nearly correct for ice clouds and introduces only a very small error (Zhang and Menzel 2002), but less so for water clouds.
- 5) *New processing software for 1-km-product generation is implemented.* Software developed for processing MODIS data at 5-km resolution could not be modified readily to generate 1-km retrievals.

2) REFINED APPROACH FOR DETERMINING LOW-LEVEL CLOUD HEIGHTS OVER OCEAN

In Collection 5, low-cloud heights are determined through comparison of the measured $11\text{-}\mu\text{m}$ BT with a vertical profile of $11\text{-}\mu\text{m}$ BTs calculated from the gridded GDAS temperature, water vapor, and ozone profiles in conjunction with the PFAAST radiative transfer model. This IR-window method finds a pressure/height level that matches the observation. It leads to biases when temperature inversions are present, with retrieved cloud heights being biased high (positive) by more than 2 km with respect to collocated CALIPSO cloud products (Holz et al. 2008). Near-surface

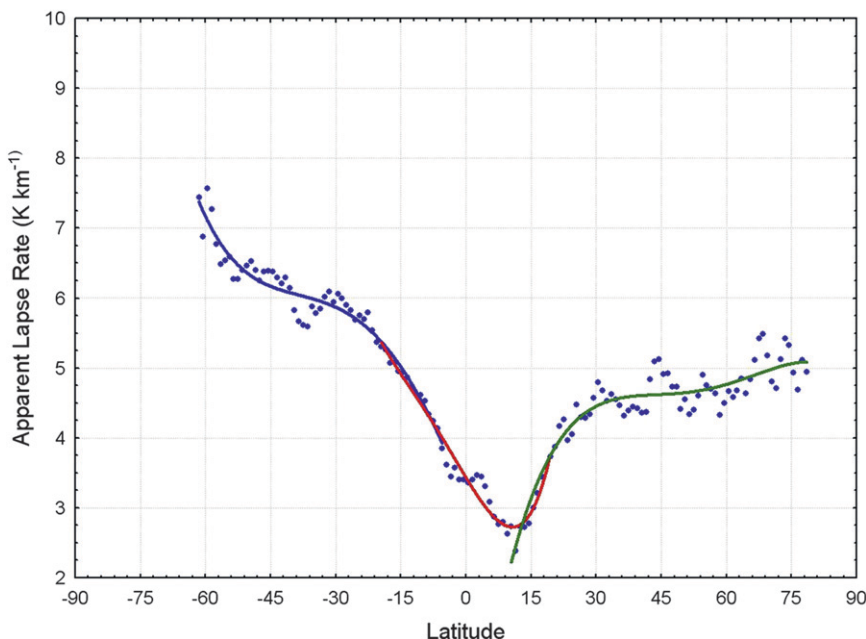


FIG. 5. Apparent lapse rates based on 11- μm BTs as a function of latitude for August. The blue points are the derived zonal-mean apparent lapse rates; the blue, red, and green lines are polynomial fits to the data. Three separate sets of regression coefficients are calculated: one each for the Southern and Northern Hemispheres and one for the tropics (blue, green, and red lines, respectively). For this month, the “break points” between the three polynomial fits are at 7.8°S and 19.5°N.

temperature inversions are common over nighttime land and in marine locations dominated by persistent stratocumulus clouds. Ancillary information from model output is often unreliable or is at coarse spatial and vertical resolutions, however, and so one cannot reliably assume that the temperature profiles will indicate the presence of inversions. To mitigate the potential presence of low-level temperature inversions, one could simply assume a lapse rate (e.g., Minnis et al. 1992), but this approach could have disadvantages for global analysis.

For Collection 6, a different technique was developed to improve marine low-cloud heights. Collocated CALIOP cloud heights, modeled and atmospherically corrected surface temperatures, and observed MODIS 11- μm BTs are combined to generate monthly zonal mean “apparent 11- μm BT lapse rates.” Because the actual boundary layer lapse rate, which may or may not include a temperature inversion, is often poorly represented in NWP profile data, the use of an apparent 11- μm BT lapse rate is an attempt to better estimate differences between the surface and measured CTTs. Low-cloud heights are calculated from the difference of the clear-sky BT and the MODIS 11- μm observed cloudy BT divided by a mean lapse rate, also called the IR-window approach (IRW). It is applied when the

CO₂-slicing algorithm is unable to retrieve a valid cloud-top pressure (insufficient cloud signal in any of the 13.3-, 13.6-, 13.9-, or 14.2- μm CO₂ absorption bands) and if the IRW method retrieval results in cloud-top pressures that are greater than 600 hPa. The IRW method will always give a result if the input radiance and atmospheric profile data are valid.

Figure 5 shows an example of the derived “apparent lapse rates” for August. The blue points are the derived zonal-mean apparent lapse rates and the blue, red, and green lines are fourth-order polynomial fits to the data. For each month of the year, three separate sets of regression coefficients were derived: one each for the tropics and the southern and northern latitudes (red, blue, and green lines, respectively). The range in latitudes that was appropriate for each set of coefficients was determined subjectively. In this case, the break points between the three latitude zones are at 7.8°S and 19.5°N. Table 1 provides a list of coefficients and break points. The predicted lapse rates are restricted to a maximum and minimum of 10 and 2 K km⁻¹, respectively. A comparison of *Aqua* MODIS with CALIOP cloud heights showed a reduction in the retrieval bias to less than 0.5 km for August of 2006.

Figure 6 shows CTH at both 5- and 1-km resolutions for the same scene shown in Fig. 4. The CTH is not

TABLE 1. Fourth-order polynomial fitting coefficients and tie points for the calculation of apparent lapse rates based on 11- μm BTs as a function of latitude for each month. For each month, the top row of coefficients is for the Southern Hemisphere (SH), the middle row is for the tropics, and the bottom row is for the Northern Hemisphere (NH). The transition from the SH to the tropics set of coefficients is given by the SH transition (latitude in degrees); likewise, the transition from the tropics to the NH sets of coefficients is given by the NH transition value (latitude in degrees).

Month	Fit	a_0	a_1	a_2	a_3	a_4	SH transition (lat)	NH transition (lat)
Jan	SH	2.976 980 1	-0.051 587 1	0.002 740 9	0.000 113 6	0.000 001 13	-3.8	22.1
	Tropics	2.942 657 7	-0.051 067 4	0.005 242 0	0.000 109 7	-0.000 003 72		
	NH	1.900 956 3	0.023 690 5	0.008 650 4	-0.000 216 7	0.000 001 51		
Feb	SH	3.348 323 9	0.137 257 5	0.013 325 9	0.000 304 3	0.000 002 19	-21.5	12.8
	Tropics	2.649 960 6	-0.010 515 2	0.004 289 6	0.000 072 0	-0.000 000 67		
	NH	2.487 873 6	-0.007 651 4	0.007 944 4	-0.000 177 4	0.000 001 15		
Mar	SH	2.406 029 6	0.037 200 2	0.009 647 3	0.000 233 4	0.000 001 65	-2.8	10.7
	Tropics	2.365 204 7	0.014 112 9	0.005 924 2	-0.000 015 9	-0.000 002 66		
	NH	3.125 127 5	-0.121 457 2	0.014 648 8	-0.000 318 8	0.000 002 10		
Apr	SH	2.652 238 7	0.032 572 9	0.010 089 3	0.000 260 1	0.000 001 99	-23.4	29.4
	Tropics	2.543 315 8	-0.004 687 6	0.005 932 5	0.000 014 4	-0.000 003 46		
	NH	13.393 170 7	-1.220 694 8	0.056 038 1	-0.000 987 4	0.000 005 98		
May	SH	1.957 826 3	-0.211 202 9	-0.005 794 4	-0.000 105 0	-0.000 000 74	-12.3	14.9
	Tropics	2.499 402 8	-0.036 470 6	0.008 200 2	0.000 084 4	-0.000 007 69		
	NH	1.643 207 0	0.115 120 7	0.003 313 1	-0.000 145 8	0.000 001 29		
Jun	SH	2.765 975 4	-0.118 650 1	0.001 162 7	0.000 093 7	0.000 001 01	-7.0	16.8
	Tropics	2.764 149 6	-0.072 862 5	0.008 887 8	0.000 176 8	-0.000 011 68		
	NH	-5.236 636 0	1.010 557 5	-0.035 544 0	0.000 518 8	-0.000 002 62		
Jul	SH	2.110 681 2	-0.307 366 6	-0.009 086 2	-0.000 089 0	0.000 000 04	-10.5	15.0
	Tropics	3.120 204 3	-0.100 237 5	0.006 405 4	0.000 262 0	-0.000 010 79		
	NH	-4.739 648 1	0.962 573 4	-0.035 584 7	0.000 552 2	-0.000 003 00		
Aug	SH	3.098 217 4	-0.162 958 8	-0.002 038 4	0.000 028 6	0.000 000 60	-7.8	19.5
	Tropics	3.433 119 5	-0.102 176 6	0.001 049 9	0.000 161 6	0.000 005 10		
	NH	-1.442 484 3	0.476 930 7	-0.013 902 7	0.000 175 9	-0.000 000 80		
Sep	SH	3.076 055 2	-0.204 346 3	-0.005 397 0	-0.000 054 1	-0.000 000 02	-8.6	17.4
	Tropics	3.453 939 0	-0.115 826 2	0.001 545 0	0.000 171 17	0.000 002 48		
	NH	-3.714 018 6	0.672 095 4	-0.021 055 0	0.000 297 4	-0.000 001 50		
Oct	SH	3.637 721 5	-0.085 778 4	0.002 431 3	0.000 149 5	0.000 001 71	-7.0	27.0
	Tropics	3.601 333 7	-0.077 580 0	0.004 194 0	0.000 094 1	-0.000 004 1		
	NH	8.223 740 1	-0.512 753 3	0.020 528 5	-0.000 301 6	0.000 001 58		
Nov	SH	3.320 616 5	-0.141 109 4	-0.002 606 8	0.000 005 8	0.000 000 42	-9.2	22.0
	Tropics	3.194 741 9	-0.104 531 6	0.004 998 6	0.000 191 1	-0.000 005 06		
	NH	-0.450 204 7	0.262 968 0	-0.001 841 9	-0.000 036 9	0.000 000 48		
Dec	SH	3.052 663 3	-0.112 152 2	-0.000 991 3	0.000 018 0	0.000 000 27	-3.7	19.0
	Tropics	3.127 637 7	-0.070 762 8	0.005 553 3	0.000 155 0	-0.000 005 71		
	NH	9.393 089 7	-0.883 668 2	0.046 045 3	-0.000 845 0	0.000 005 18		

a parameter provided in Collection 5. At both 1- and 5-km resolutions, the low-level clouds are calculated using the predicted lapse rate and the mid- to high-level cloud heights are obtained using the SRF shifts discussed earlier. For the southeastern portion of the image, note that the CTH values are somewhat affected by the input gridded meteorological profiles; this impact is not as obvious in the 1-km product.

3) UPPER-TROPOSPHERE/LOWER-STRATOSPHERE CLOUD DETECTION

The ability to infer CTH can be problematic near the tropopause where there is little if any temperature gradient. The upper boundary for CTH is dependent on the location of the tropopause as indicated by the

meteorological profiles provided by the GDAS product. Detection of UT/LS clouds is accomplished by determining when a measurement from a highly absorbing band, such as from a band that is sensitive to water vapor or carbon dioxide, is warmer than a less-absorbing band. The primary consideration is that there is a high-level temperature inversion indicated by the measurements. Radiative transfer model simulations (not shown) show that when BTs increase as spectral bands become more absorbing it is indicative of a cloud residing within 2 km of the tropopause, either in the upper troposphere or in the lower stratosphere.

Early work focused on radiation at 6.7 μm when absorbed by the water vapor at the cloud top and re-emitted at higher stratospheric temperatures. Soden

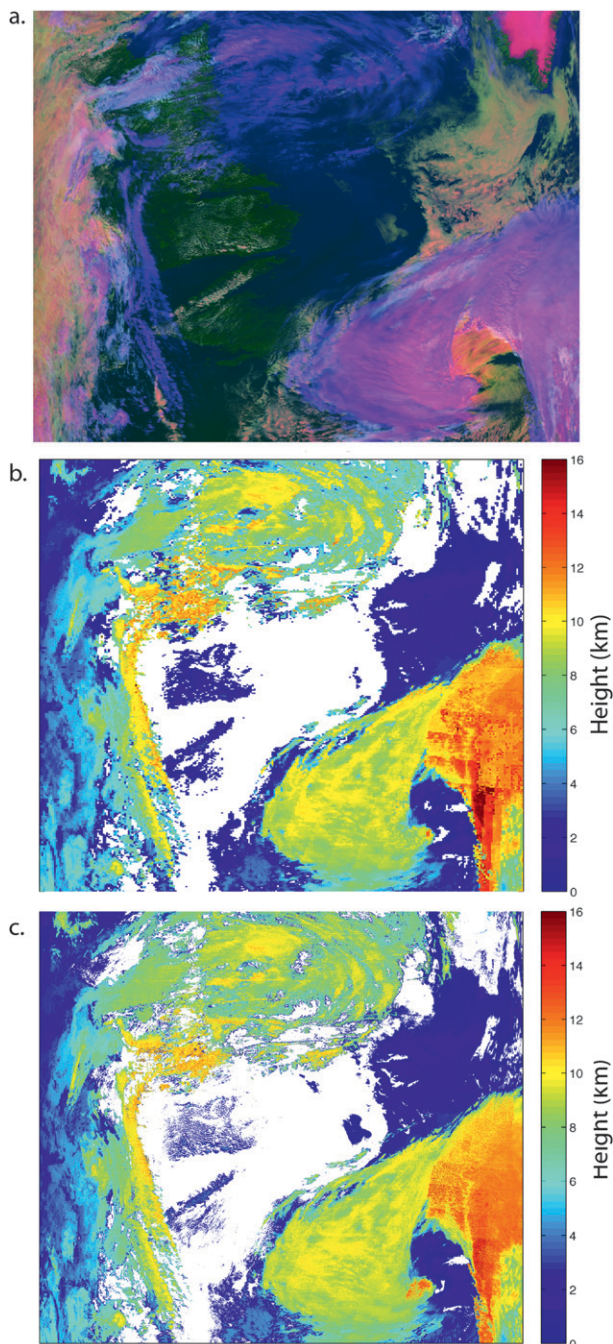


FIG. 6. For a MODIS granule at 1630 UTC 28 Aug 2006, over the northern Atlantic Ocean, (a) a false-color image (red, 0.65 μm ; green, 2.15 μm ; blue, 11 μm reversed) in which ocean is dark, land is green, cirrus is blue, optically thick ice cloud is magenta, and low clouds are yellow/white, and MODIS CTHs at (b) 5- and (c) 1-km resolution.

and Bretherton (1993) explained that under clear-sky conditions radiation at 6.7 μm is primarily absorbed by water vapor and emitted in the atmospheric layer between 200 and 500 hPa while radiation at 11 μm is

from the surface, with a slight attenuation from the near-surface water vapor. Because the surface is usually warmer than the higher levels of the atmosphere, it is expected that $BT(11 \mu\text{m}) > BT(6.7 \mu\text{m})$. For an opaque cloud located at the tropopause or higher, a measurement at 6.7 μm is affected by whatever water vapor is present above the cloud, which acts to increase the measured radiance and hence BT at this wavelength. The $BT(11 \mu\text{m})$ is more representative of an opaque cloud that is much colder than the surrounding atmosphere in the lower stratosphere. In this case, the $BT(6.7 \mu\text{m}) > BT(11 \mu\text{m})$. The $BTD(6.7-11)$ depends on the amount of water vapor above the cloud and the temperature lapse rate in the stratosphere. Ackerman (1996) noted that $BTD(6.7-11) > 0$ when the field of view is partially cloudy for very cold clouds; he suggested that differences of less than 2 K could be attributed to nonuniform fields of view. Schmetz et al. (1997) studied stratospheric clouds by using Meteosat water vapor and IR-channel observations and used the test $BTD(6.7-11) + 1 \text{ K}$.

For MODIS detection of UT/LS clouds, pixels are flagged in which $BT(13.9 \mu\text{m}) > BT(13.3 \mu\text{m}) + 0.5 \text{ K}$. The $BTD(13.9-13.3)$ depends on the amount of CO_2 above the cloud and the lapse rate in the stratosphere. Because CO_2 remains relatively uniform, this test is seemingly more robust than the $BTD(6.7-11)$ test. An example of the UT/LS cloud detection is presented in Fig. 7 for a granule over the Indian Ocean at 0800 UTC 26 August 2006. The grayscale image is provided from MODIS band 36 at 14.2 μm ; the pixels painted in red are those for which UT/LS clouds were detected.

A more detailed examination of the effectiveness and robustness of this test is provided in section 5 through comparison of CALIOP and MODIS cloud products.

4. Global results

a. Nearest-neighbor gridding approach

To compare a day of global data from one sensor with that from another, it can be very useful to adopt a common grid, especially when the two sensors have different spatial resolutions. The approach used in this study is to subsample the level 2 data (pixel-level products) and to place them onto an equal-angle grid (see Fig. 8). This implementation finds the pixel that is closest to a grid point and “snaps” the information associated with that pixel to that grid point; that is, the procedure uses a nearest-neighbor approach. If, on a subsequent overpass, another pixel is found that is close to the grid point, the pixel that has the smallest scan angle is chosen; that is, the pixel that is closest to nadir is chosen. This is more

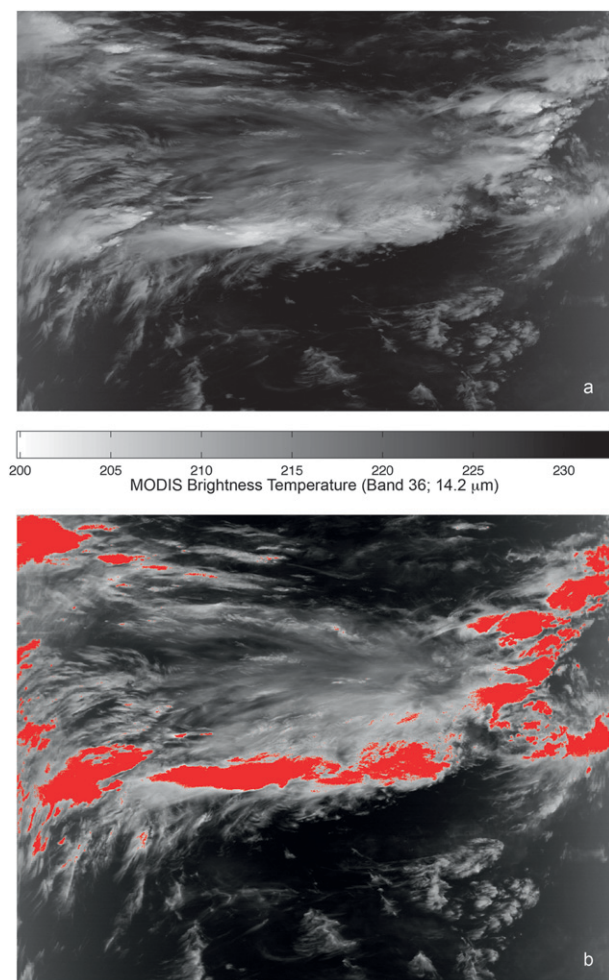


FIG. 7. Detection of clouds in the UT/LS for a MODIS granule at 0800 UTC 28 Aug 2006, over the Indian Ocean: (a) BTs (K) for MODIS band 36 ($14.2 \mu\text{m}$) and (b) pixels identified with the stratospheric cloud test shown painted in red.

likely to occur at high latitudes when there are multiple overpasses over a given location over the course of a day.

b. MODIS IR thermodynamic cloud phase

Results are shown in Fig. 9 for daytime IR-phase results at a grid resolution of 0.2° . Figure 9a shows the result from application of the Collection-5 threshold tests, and Fig. 9b shows results from application of the new algorithm shown in Fig. 3. For the Collection-5 results, pixels that are not positively identified as either ice or water are labeled as uncertain. Note that pixels that were previously classified as uncertain are now classified more often as containing ice clouds. There is still no attempt to classify cloud pixels as perhaps having a lower-level water-cloud layer underneath the ice layer.

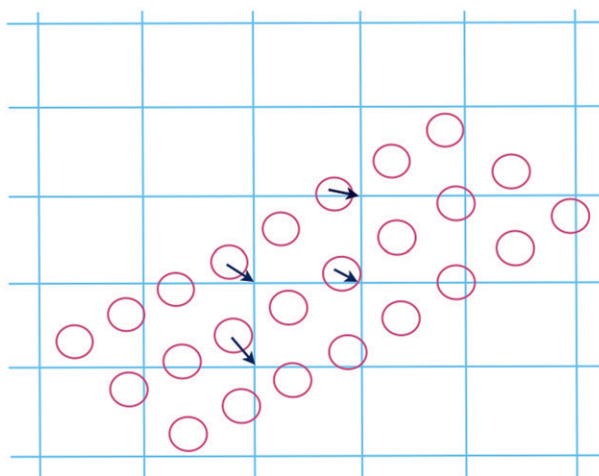


FIG. 8. Cartoon depicting how imager pixels (red circles) are “snapped” (follow the black arrows) onto an equal-angle grid (in blue) using a nearest-neighbor approach.

Phase discrimination for supercooled water clouds remains problematic.

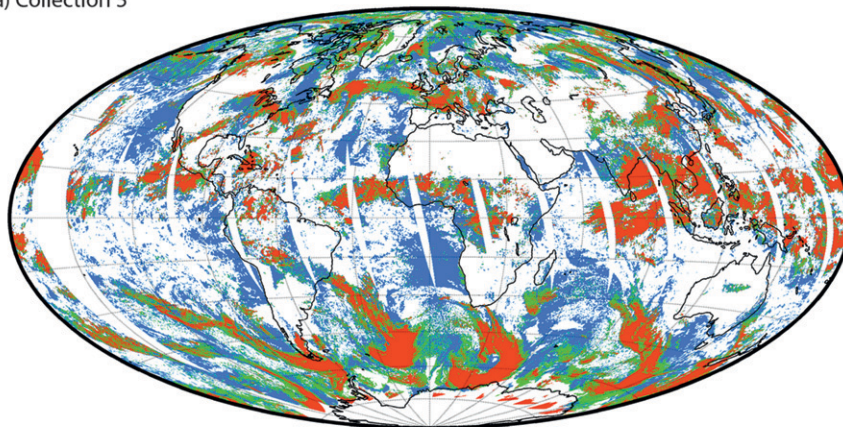
c. MODIS cloud-top height/pressure/temperature

The Collection-5 (C5 and earlier) cloud products did not have CTH as an explicit parameter, an oversight that is remedied in both the 1- and 5-km Collection-6 (C6) products. Collection-6 CTHs at 5- and 1-km spatial resolutions are shown in Fig. 10. The primary differences are due to the cloud mask: low clouds do not appear to be as blocky in the 1-km results. While not evident in the global image, another primary difference is that the heights for high-level clouds do not vary near the cloud edges where the opacity drops significantly: the cloud heights are stable even at low cloud opacities.

5. Comparison of CALIOP and MODIS Collection-6 cloud properties

As discussed in Holz et al. (2008), MODIS to CALIOP collocation files are prepared for data products from each MODIS granule. These collocation files can be analyzed to produce global comparison statistics. Figure 11a shows the gridded mean values of the (MODIS C5–CALIOP) CTH differences for August 2006, at 5° resolution in latitude and longitude between 60°N and 60°S , with both sensor products at 5-km spatial resolution. The (MODIS C5–CALIOP) CTH differences are limited to single-layered clouds as determined by CALIOP. Similar results are provided in Fig. 11b for (MODIS C6–CALIOP) CTH values. The most notable improvement in the (MODIS C6–CALIOP) CTH comparison (Fig. 11b) is the reduction in positive values

a) Collection 5



b) Collection 6

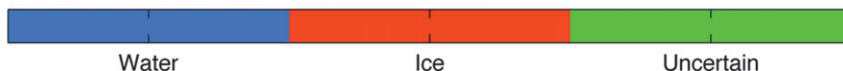
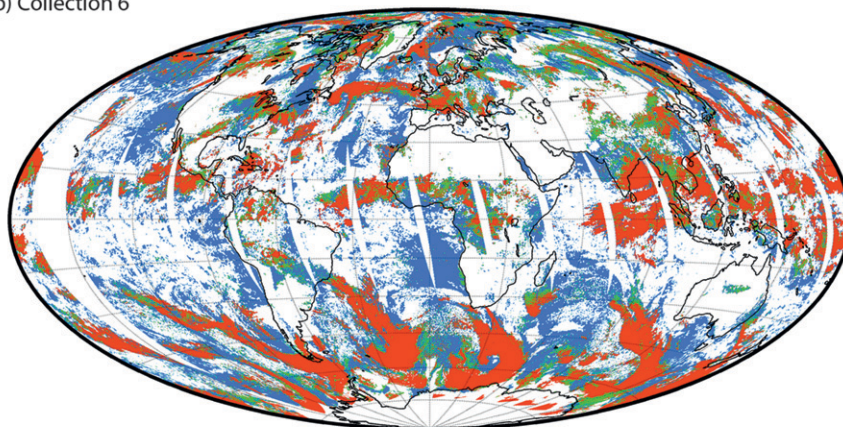


FIG. 9. Snap-to-grid results for daytime IR cloud phase on 28 Aug 2006 for (a) the Collection-5 IR-phase algorithm and (b) the improved IR cloud phase. For the Collection-5 results, the mixed-phase pixels are merged into the uncertain category, as will be done with Collection 6.

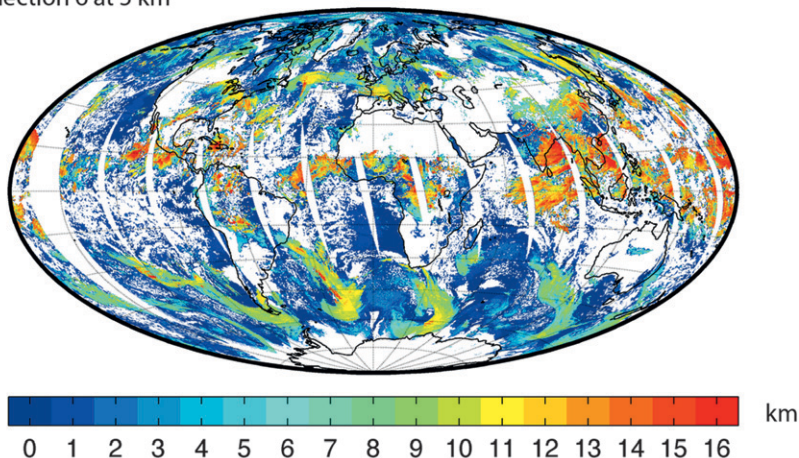
of (MODIS–CALIOP) CTH differences; this is a result of applying the new lapse-rate approach for estimating low-cloud CTH in the MODIS data (Holz et al. 2008). The nonpolar low-cloud height (CALIOP CTH < 3 km) bias of 424 m for Collection 5 was reduced to 197 m for Collection 6.

Another way of comparing the MODIS and CALIOP CTHs is provided in Fig. 12, which shows the CTH differences between the MODIS C5/C6 and CALIOP products, again with both sensor products at 5-km spatial resolution. The percentages are calculated at a resolution of 0.1-km CTH difference; integration of the percentages in each panel sums to 100%. Figure 12a filters the total number of MODIS and CALIOP matchups for August 2006 between 60°N and 60°S for single-layered cirrus over both ocean and land. The single-layered cirrus is defined when two conditions are

met: 1) CALIOP CTH ≥ 8 km and 2) CALIOP sees the surface. For this month, a total of 54 992 MODIS–CALIOP collocations met these conditions. There are two features to note in Fig. 12a. First, the (MODIS–CALIOP) CTH differences occurring between –7 and –12 km (i.e., high cloud being miscast as low cloud by MODIS) decreased for the C6 product. Second, the peak for C6 near a value of –1 km is higher than for the C5 results. Some differences in (MODIS–CALIOP) CTH are expected since MODIS sees into the cloud to an optical thickness of approximately 1 while CALIOP senses the cloud top (Holz et al. 2008). Together, these results indicate that CO₂ slicing is being used more often, and to greater advantage, with the C6 algorithm than occurred with C5.

Figure 12b shows the differences for low-level clouds over ocean between 60°N and 60°S (i.e., clouds within

a) Collection 6 at 5 km



b) Collection 6 at 1 km

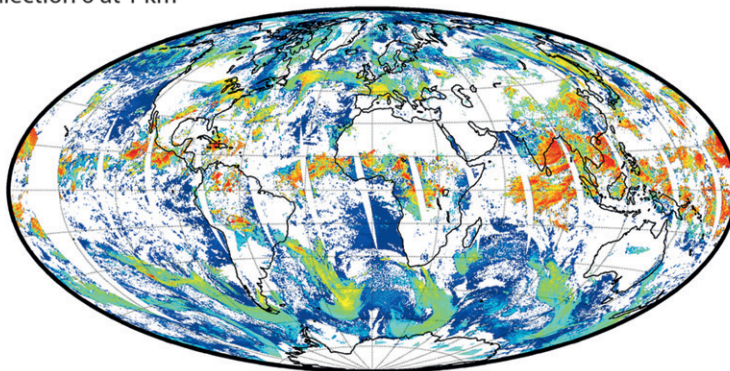


FIG. 10. Snap-to-grid results for daytime CTH on 28 Aug 2006, for Collection 6 at (a) 5- and (b) 1-km resolutions.

3 km of the surface). For this comparison, there were 259 209 collocations between MODIS and CALIOP. The (MODIS C5–CALIOP) results show the presence of a peak between 1 and 2 km. As shown previously, this tends to occur in the presence of temperature inversions. With use of the lapse-rate approach, the (MODIS C6–CALIOP) CTH differences no longer display this secondary peak.

Cloud thermodynamic phase retrievals from both MODIS and CALIOP (Hu et al. 2009) are presented as the likelihood of inferring water/ice phase as a function of CALIOP mean cloud temperature, following Giraud et al. (2001; see Fig. 12). The results in Giraud et al. (2001) are based on collocated products from the Polarization and Directionality of the Earth's Reflectance (POLDER) radiometer and the Along-Track Scanning Radiometer (ATSR-2). POLDER data provide the cloud thermodynamic phase by following the method of Riedi et al. (2000), and the ATSR-2 data are analyzed to provide the cloud-top temperature (CTT). Their results over ocean indicated that the likelihood of finding ice

clouds is less than 5% for $CTT \geq 268$ K and greater than 95% for $CTT \leq 238$ K. As CTT decreases from 268 to 238 K, the likelihood of finding an ice cloud increases while following a nearly linear relationship.

Both MODIS and CALIOP products are filtered so that results are shown only for collocations where CALIOP data indicate single-layered clouds and an optical thickness $\tau \geq 0.5$. At each CALIOP mean cloud temperature, the CALIOP or MODIS cloud-phase retrievals at that temperature are normalized so that the percentages of each category (water, ice, and uncertain) sum to 100%. Figures 13a and 13b show the results from CALIOP for ocean and land, respectively. The CALIOP ice–water phase confidence flags were not used to filter the results—all data were used. After filtering the CALIOP results for single-layered clouds and leaving out the most optically thin clouds, there are only a few percent of uncertain retrievals in the CALIOP version-3 products except at warm cloud temperatures above 285 K over land. This indicates that CALIOP is able to infer the presence of ice or water clouds fairly

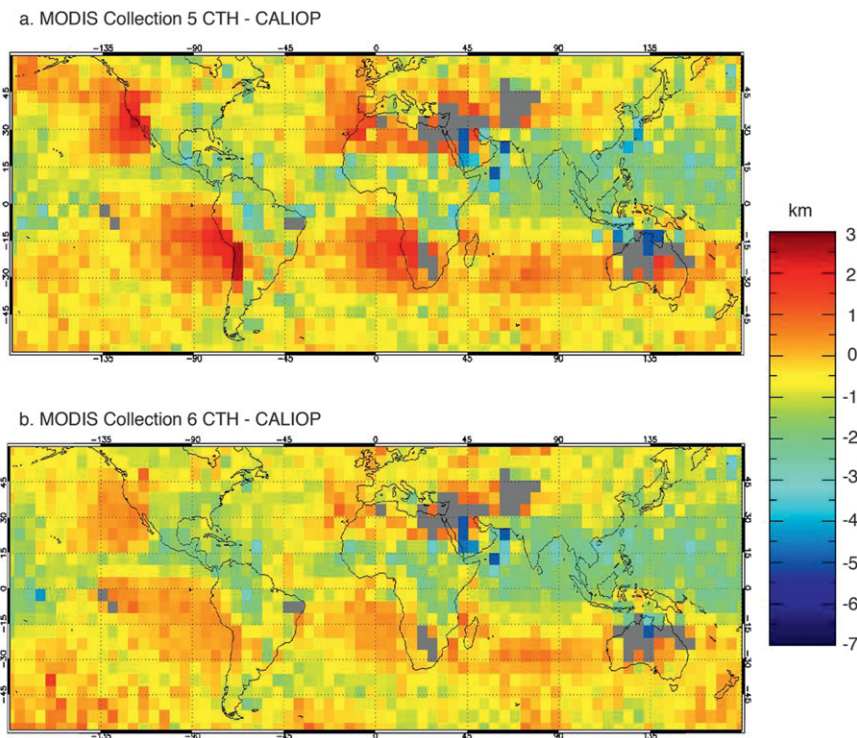


FIG. 11. Comparison of mean CTH differences for collocations between MODIS and CALIOP products for August 2006. The individual collocation CTH differences are averaged in grid cells at 5° resolution in latitude and longitude between 60°N and 60°S . The results are filtered for single-layered clouds that have an optical thickness of ≥ 0.5 as determined from the CALIOP version-3 product.

unambiguously. Over both land and ocean, it is somewhat surprising to find that CALIOP infers the presence of a high percentage of water clouds even at cloud temperatures below 250 K. These results are supported by Hu et al. (2010) in a study on supercooled water clouds that used CALIOP data. Over land, where there are supposedly higher concentrations of ice nuclei, the percentage of supercooled water clouds decreases with mean cloud temperature in comparison with the results over ocean.

In comparison with the CALIOP results, the MODIS results shown in Figs. 13c and 13d over ocean and land, respectively, both indicate much higher percentages of pixels for which the cloud-phase retrieval is uncertain, especially between 240 and 260 K. While the improvements in the MODIS cloud-phase algorithm presented in this study pertain mostly to optically thin ice clouds, the ability to infer the presence of supercooled water clouds is problematic using only IR bands (Nasiri and Kahn 2008; Cho et al. 2009). The results for MODIS are provided as a function of CALIOP mean cloud temperature and not optical thickness; the results include retrievals over a range of cloud optical thicknesses. Note

that the use of the emissivity ratios over land for the MODIS cloud phase are influenced to some degree by the quality of the surface temperature provided by the meteorological-model product.

MODIS and CALIOP collocations for August 2006 are also used to examine the detection of UT/LS clouds determined by the simple BT(13.9–13.3 μm) test discussed in section 3c(3). The collocated CALIOP–MODIS data are studied to determine both the effectiveness of this test and also the robustness of the threshold adopted to identify these pixels. Figure 14 shows a histogram on a \log_{10} scale of the difference between the CALIOP CTH and the tropopause height as a function of the BT(13.9–13.3 μm). In this analysis, the tropopause height for each collocated point is based on the temperature profile provided in the GDAS meteorological product. Data for both daytime and nighttime collocations are used over all surface types, but the data are limited to the latitude range between 60°S and 60°N .

The collocated observations considered for analysis were ones for which both CALIOP and MODIS detected clouds, for which CALIOP reported cloud heights below 20 km, and for which CALIOP determined that the

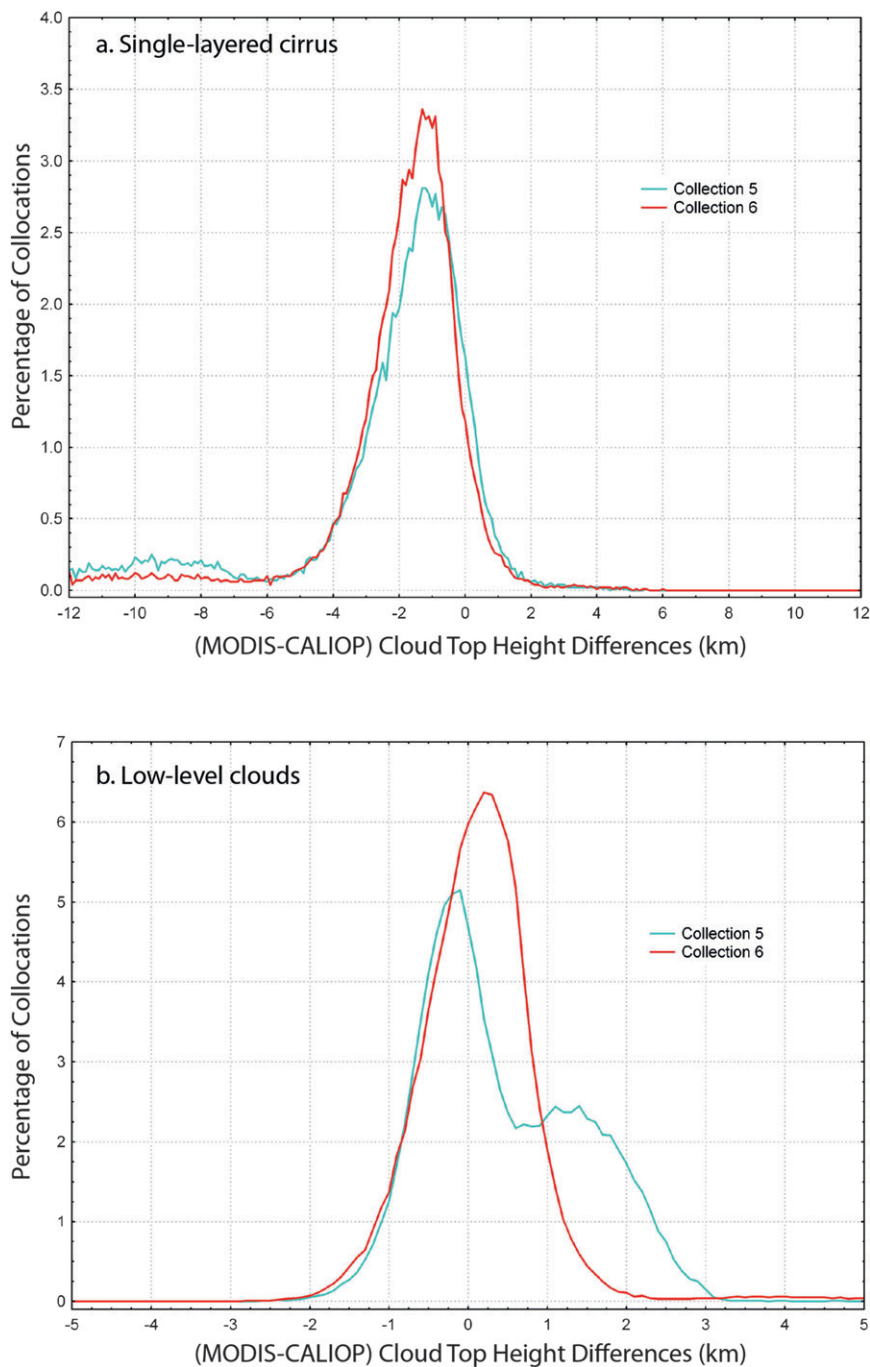


FIG. 12. CTH differences for collocations between MODIS and CALIOP products for August 2006. The individual MODIS–CALIOP collocations are filtered for (a) single-layered cirrus and (b) low-level clouds. The single-layered cirrus is defined when two conditions are met: 1) CALIOP CTH ≥ 8 km and 2) CALIOP sees the surface. A total of 54 992 MODIS–CALIOP collocations met these conditions for single-layered cirrus for August 2006. Low-level clouds were determined from CALIOP, and there were 259 209 total collocations for the same month. The percentages are calculated at a resolution of 0.1-km CTH difference.

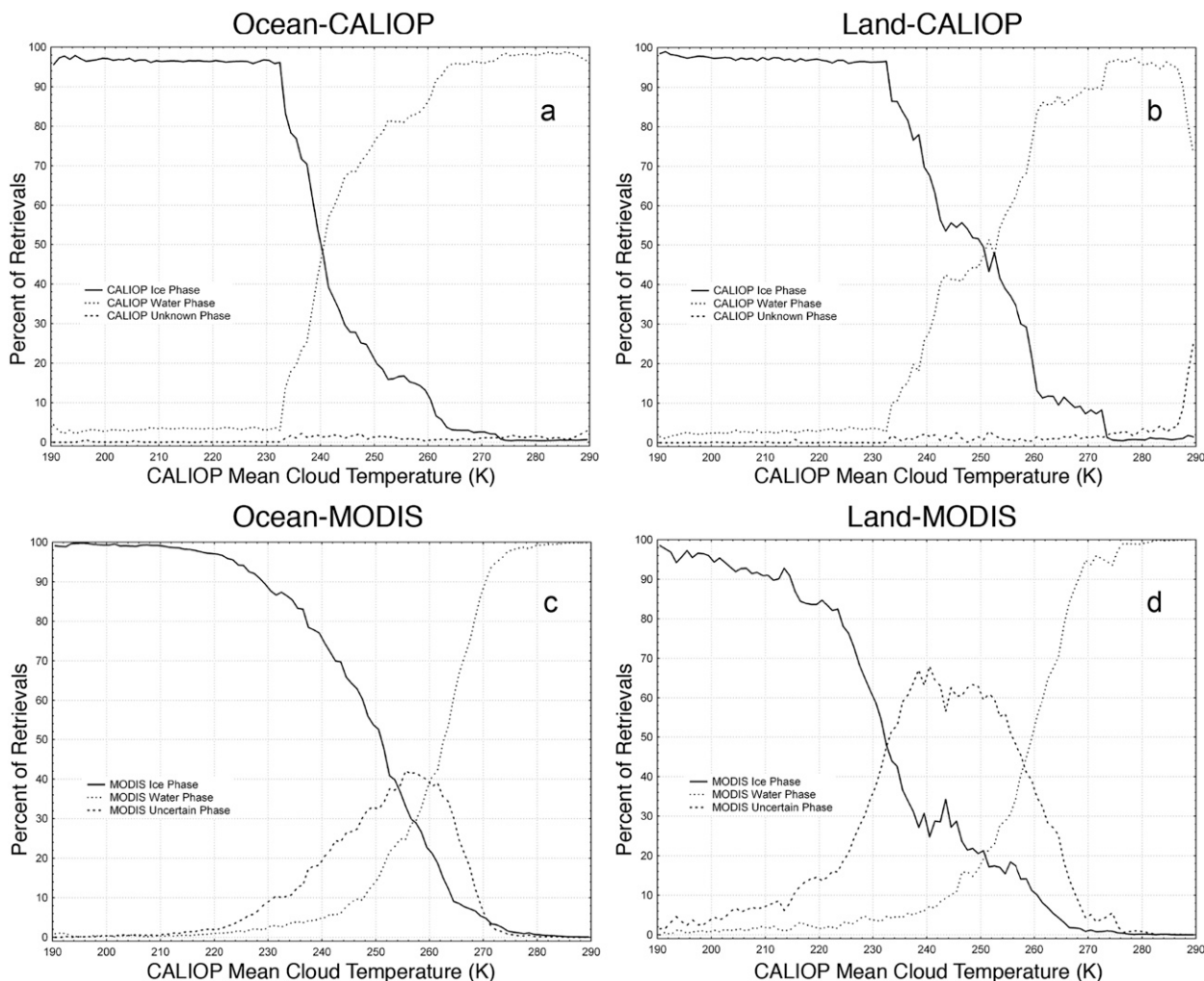


FIG. 13. Likelihood of inferring the presence of ice or water cloud as a function of CTT in the pixel collocations between MODIS and CALIOP for August 2006. The results are filtered to observations of single-layered clouds that have an optical thickness > 0.5 as determined from the CALIOP version-3 product. CALIOP cloud phase is presented as a function of CALIOP mean cloud temperature over (a) ocean and (b) land. For comparison, MODIS cloud phase is presented as a function of CALIOP mean cloud temperature over (c) ocean and (d) land. Note that CALIOP has a class called “unknown” in the version-3 data product while MODIS uses the term uncertain.

clouds were single layered and continuous over 5-km areas. With these requirements, a total of 3 963 859 cloud collocations were found for the month. The percentage of these clouds higher than 8 km as measured by CALIOP was 31% while MODIS found 32% at these levels. CALIOP found 21% of the nearly four million single-layer and overcast scenes to be within 2 km of the tropopause (UT/LS clouds). Application of the MODIS $BTD(13.9-13.3) > 0.5$ K test yielded 78 164 UTLS cloudy pixels. For virtually all of these clouds, CALIOP measured optical depths of ≥ 1 ; 96% of the CALIOP cloud heights were within 2 km of the tropopause, as were 89% of the MODIS cloud heights.

Although fewer MODIS pixels will be flagged if the $BTD(13.9-13.3)$ threshold is increased, our testing indicates that the chosen pixels still tend to identify coherent regions in a given MODIS granule as shown in Fig. 7. For this month of collocated CALIOP–MODIS products, the MODIS $BTD(13.9-13.3)$ test is found to reliably identify clouds that reside in the UT/LS.

6. Summary and conclusions

This paper summarizes the refinements in the MODIS operational cloud-top property algorithms implemented for MODIS Collection 6. The improvement in the products is a result of both algorithm and calibration improvements,

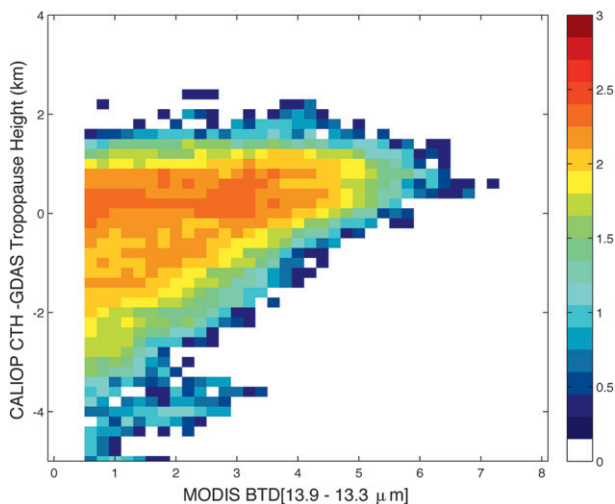


FIG. 14. Histogram of collocations between CALIOP version-3 5-km and MODIS Collection-6 1-km products for August 2006: MODIS BTD(13.9–13.3) is shown as a function of the difference between the CALIOP CTH and the tropopause height. The tropopause height is determined from the temperature profiles in the GDAS model at the closest time and location to the MODIS data. The collocated data are from 60°S to 60°N for both daytime and nighttime conditions over all surfaces but are filtered for single-layered, overcast clouds (CALIOP quality-control flag ≥ 18). The color is in \log_{10} scale.

resulting in the future availability of cloud macrophysical properties at 1-km spatial resolution, including cloud-top pressure and temperature and IR cloud thermodynamic phase. In addition, new parameters for Collection 6 include cloud-top height and a flag for clouds in the upper troposphere/lower stratosphere, that is, a cloud within ± 2 km of the tropopause.

The Collection-6 development activities were influenced primarily by 1) improved characterization of the MODIS spectral response functions for the 15- μm CO_2 bands achieved through comparison with AIRS high-spectral-resolution infrared data and 2) repeated comparison of global MODIS and CALIPSO instantaneous cloud products throughout the course of algorithm refinement. The comparison of MODIS with AIRS radiances enabled both finding and mitigating biases in some of the MODIS IR bands that are most important for cloud-height retrievals. The cause of these biases is unknown, but a single small adjustment in the MODIS SRFs is found to mitigate most of the effects. Whereas the cloud-top macrophysical parameters were provided through Collection 5 solely at 5-km spatial resolution, Collection 6 also offers these parameters at 1-km spatial resolution.

One of the most useful findings during the development process for MODIS Collection-6 activities is the ability to modify an algorithm, conduct tests on global data, and

subsequently build collocation files between MODIS and CALIOP products. As shown in Holz et al. (2008) and Menzel et al. (2008), such collocation files are critical for finding biases in cloud properties for various cloud types such as thin cirrus and supercooled water clouds. Such an approach will remain a critical part of any subsequent calibration and validation activities. On the basis of the comparisons with CALIOP, the Collection-6 MODIS CTH biases for low-level boundary layer water clouds are reduced considerably from 424 m for Collection 5 to 197 m for Collection 6. The CALIOP version-3 products were likewise useful for evaluating improvements to the MODIS IR-phase algorithm. As a result, the MODIS Collection-6 phase algorithm no longer includes a class for supercooled/mixed-phase clouds and will present these cases as being of uncertain phase. The ability of the Collection-6 IR-phase algorithm to infer the phase of optically thin ice clouds is improved, but problematic phase determination for supercooled water clouds remains an open issue. As shown by the CALIOP phase product, high percentages of supercooled water clouds can exist even at very cold temperatures below 250 K.

Acknowledgments. This work is funded through NASA Grant NNX11AH62G. The team at the Atmosphere PEATE was instrumental in providing computational and logistical support; we are grateful for their contributions. We thank Fred Nagle for developing the software to collocate data between the various A-Train sensors. The authors also acknowledge the three reviewers who provided invaluable comments that helped us improve the manuscript. The views, opinions, and findings contained in this report are those of the author(s) and should not be construed as an official National Oceanic and Atmospheric Administration or U.S. government position, policy, or decision.

REFERENCES

- Ackerman, S. A., 1996: Global satellite observations of negative brightness temperature differences between 11 and 6.7 μm . *J. Atmos. Sci.*, **53**, 2803–2812.
- , R. E. Holz, R. Frey, E. W. Eloranta, B. C. Maddux, and M. McGill, 2008: Cloud detection with MODIS. Part II: Validation. *J. Atmos. Oceanic Technol.*, **25**, 1073–1086.
- Aumann, H. H., and Coauthors, 2003: AIRS/AMSU/HSB on the Aqua mission: Design, science objectives, data products, and processing systems. *IEEE Trans. Geosci. Remote Sens.*, **41**, 253–264.
- Chahine, M. T., and Coauthors, 2006: The Atmospheric Infrared Sounder (AIRS): Improving weather forecasting and providing new insights into climate. *Bull. Amer. Meteor. Soc.*, **87**, 911–926.
- Cho, H.-M., S. L. Nasiri, and P. Yang, 2009: Application of CALIOP measurements to the evaluation of cloud phase

- derived from MODIS infrared channels. *J. Appl. Meteor. Climatol.*, **48**, 2169–2180.
- Derber, J. C., D. F. Parrish, and S. J. Lord, 1991: The new global operational analysis system at the National Meteorological Center. *Wea. Forecasting*, **6**, 538–547.
- Frey, R. A., S. A. Ackerman, Y. Liu, K. I. Strabala, H. Zhang, J. R. Key, and X. Wang, 2008: Cloud detection with MODIS. Part I: Improvements in the MODIS cloud mask for Collection 5. *J. Atmos. Oceanic Technol.*, **25**, 1057–1072.
- Giraud, V., O. Thouron, J. Riedi, and P. Goloub, 2001: Analysis of direct comparison of cloud top temperature and infrared split window signature against independent retrievals of cloud thermodynamic phase. *Geophys. Res. Lett.*, **28**, 983–986.
- Heidinger, A. K., and M. J. Pavolonis, 2009: Gazing at cirrus clouds for 25 years through a split window. Part I: Methodology. *J. Appl. Meteor. Climatol.*, **48**, 1100–1116.
- , —, R. E. Holz, B. A. Baum, and S. Berthier, 2010: Using CALIPSO to explore the sensitivity to cirrus height in the infrared observations from NPOESS/VIIRS and GOES-R/ABI. *J. Geophys. Res.*, **115**, D00H20, doi:10.1029/2009JD012152.
- Holz, R. E., S. A. Ackerman, F. W. Nagle, R. Frey, S. Dutcher, R. E. Kuehn, M. Vaughan, and B. A. Baum, 2008: Global MODIS cloud detection and height evaluation using CALIOP. *J. Geophys. Res.*, **113**, D00A19, doi:10.1029/2008JD009837.
- Hu, Y.-X., and Coauthors, 2009: CALIPSO/CALIOP cloud phase discrimination algorithm. *J. Atmos. Oceanic Technol.*, **26**, 2293–2309.
- , S. Rodier, K.-M. Xu, W. Sun, J. Huang, B. Lin, P. Zhai, and D. Josset, 2010: Occurrence, liquid water content, and fraction of supercooled water clouds from combined CALIOP/IIR/MODIS measurements. *J. Geophys. Res.*, **115**, D00H34, doi:10.1029/2009JD012384.
- Menzel, W. P., and Coauthors, 2008: MODIS global cloud-top pressure and amount estimation: Algorithm description and results. *J. Appl. Meteor. Climatol.*, **47**, 1175–1198.
- Minnis, P., P. W. Heck, D. F. Young, C. W. Fairall, and J. B. Snider, 1992: Stratocumulus cloud properties derived from simultaneous satellite and island-based instrumentation during FIRE. *J. Appl. Meteor.*, **31**, 317–339.
- Moody, E. G., M. D. King, and S. Platnick, 2005: Spatially complete global spectral albedos: Value-added datasets derived from Terra MODIS land products. *IEEE Trans. Geosci. Remote Sens.*, **43**, 144–158.
- Nasiri, S. L., and B. H. Kahn, 2008: Limitations of bispectral infrared cloud phase determination and potential for improvement. *J. Appl. Meteor. Climatol.*, **47**, 2895–2910.
- Parol, F., J. Buriez, G. Brogniez, and Y. Fouquart, 1991: Information content of AVHRR channels 4 and 5 with respect to the effective radius of cirrus cloud particles. *J. Appl. Meteor.*, **30**, 973–984.
- Pavolonis, M. J., 2010: Advances in extracting cloud composition information from spaceborne infrared radiances—A robust alternative to brightness temperatures. Part I: Theory. *J. Appl. Meteor. Climatol.*, **49**, 1992–2012.
- Pinty, B., and M. M. Verstraete, 1992: GEMI: A non-linear index to monitor global vegetation from satellites. *Vegetatio*, **101**, 15–20.
- Platnick, S., M. D. King, S. A. Ackerman, W. Paul Menzel, B. A. Baum, and R. A. Frey, 2003: The MODIS cloud products: Algorithms and examples from Terra. *IEEE Trans. Geosci. Remote Sens.*, **41**, 459–473.
- Riedi, J., M. Doutriaux-Boucher, P. Goloub, and P. Couvert, 2000: Global distribution of cloud top phase from POLDER/ADEOS-1. *Geophys. Res. Lett.*, **27**, 1707–1710.
- Salomonson, V. V., W. L. Barnes, P. W. Maymon, H. E. Montgomery, and H. Ostrow, 1989: MODIS: Advanced facility instrument for studies of the earth as a system. *IEEE Trans. Geosci. Remote Sens.*, **27**, 145–153.
- Schmetz, J., S. A. Tjemkes, M. Gube, and L. van de Berg, 1997: Monitoring deep convection and convective overshooting with Meteosat. *J. Adv. Space Res.*, **10**, 433–441.
- Schreier, M. M., B. H. Kahn, A. Eldering, D. A. Elliott, E. Fishbein, F. W. Irion, T. S. Pagano, 2010: Radiance comparisons of MODIS and AIRS using spatial response information. *J. Atmos. Oceanic Technol.*, **27**, 1331–1342.
- Seemann, S. W., E. E. Borbas, R. O. Knuteson, G. R. Stephenson, and H.-L. Huang, 2008: Development of a global infrared land surface emissivity database for application to clear sky sounding retrievals from multispectral satellite radiance measurements. *J. Appl. Meteor. Climatol.*, **47**, 108–123.
- Soden, B. J., and F. B. Bretherton, 1993: Upper tropospheric relative humidity from the GOES 6.7 μm channel: Method and climatology for July 1987. *J. Geophys. Res.*, **98**, 16 669–16 688.
- Strow, L. L., S. Hannon, S. Machado, H. Motteler, and D. Tobin, 2003: An overview of the AIRS radiative transfer model. *IEEE Trans. Geosci. Remote Sens.*, **41**, 303–313.
- , S. E. Hannon, S. De-Souza Machado, H. E. Motteler, and D. C. Tobin, 2006: Validation of the Atmospheric Infrared Sounder radiative transfer algorithm. *J. Geophys. Res.*, **111**, D09S06, doi:10.1029/2005JD006146.
- Susskind, J., C. D. Barnett, and J. M. Blaisdell, 2003: Retrieval of atmospheric and surface parameters from AIRS/AMSU/HSB data in the presence of clouds. *IEEE Trans. Geosci. Remote Sens.*, **41**, 390–409.
- Tobin, D. C., and Coauthors, 2006a: Radiometric and spectral validation of Atmospheric Infrared Sounder observations with the aircraft-based Scanning High-Resolution Interferometer Sounder. *J. Geophys. Res.*, **111**, D09S02, doi:10.1029/2005JD006094.
- , H. E. Revercomb, C. C. Moeller, and T. S. Pagano, 2006b: Use of Atmospheric Infrared Sounder high-spectral resolution spectra to assess the calibration of Moderate Resolution Imaging Spectroradiometer on EOS Aqua. *J. Geophys. Res.*, **111**, D09S05, doi:10.1029/2005JD006095.
- Winker, D. M., W. H. Hunt, and M. J. McGill, 2007: Initial performance assessment of CALIOP. *Geophys. Res. Lett.*, **34**, L19803, doi:10.1029/2007GL030135.
- , M. A. Vaughan, A. Omar, Y. Hu, K. A. Powell, Z. Liu, W. H. Hunt, and S. A. Young, 2009: Overview of the CALIPSO mission and CALIOP data processing algorithms. *J. Atmos. Oceanic Technol.*, **26**, 2310–2323.
- Xiong, X., B. N. Wenny, and W. L. Barnes, 2009: Overview of NASA Earth Observing Systems Terra and Aqua Moderate Resolution Imaging Spectroradiometer Instrument calibration algorithms and on-orbit performance. *J. Appl. Remote Sens.*, **3**, 032501, doi:10.1117/1.3180864.
- Zhang, H., and W. P. Menzel, 2002: Improvement in thin cirrus retrievals using an emissivity adjusted CO₂ slicing algorithm. *J. Geophys. Res.*, **107**, 4327–4340.